IAC-14-C4.2.9 x 24281

AN ADVANCED HYBRID ROCKET ENGINE FOR AN ALTERNATIVE UPPER STAGE OF THE BRAZILIAN VLM 1 LEO-LAUNCHER

Ognjan Božić*
Ognjan.bozic@dlr.de

Georg Poppe* and Dennis Porrmann*
georg.poppe@dlr.de dennis.porrman@dlr.de

*German Aerospace Center (DLR),
Institute of Aerodynamics and Flow Technology, Braunschweig, Germany,

The Institute of Aeronautics and Space (IAE), on behalf of the Brazilian Space Agency (AEB), is developing a new launch system called Microsatellite Launch Vehicle (VLM-1). The development is supported by German Aerospace Center (DLR) and some German industrial companies. Basically, the VLM-1 is planned as a three stage launcher with solid rocket engines, which could deliver up to 200 kg payload in Low Earth Orbit (LEO). To propel the 1st and 2nd stage the launcher will be equipped with solid rocket engines of the type S50, which have identical structure for both stages. The only exception is a different nozzle expansion ratio. As a 3rd stage the solid rocket engine S44 combined with attached RCS system, based on cold gas engines, is planned. To overcome the maneuverability limitations at injection phase of payload into LEO, an alternative hybrid rocket engine (HRE) for the 3rd stage is analyzed by the Institute of Aerodynamics and Flow Technology of DLR Braunschweig. As a suitable propellant mixture for this engine High Test Peroxide (HTP) is selected as oxidizer, with concentrations higher than 87.5 wt%, and polymeric hydrocarbon fuels with different ingredients, which improves the regression rate and combustion efficiency. One of the analyzed propellant mixtures is verified in experiments carried out within the DLR AHRES program (Advanced Hybrid Rocket Engine Simulation) on the test facility Trauen, Germany. In this paper the predesign of the HRE concept possesses the ability of multi-ignition, due to a catalyst for the decomposition of hydrogen peroxide (HTP), throttle-ability in the range 1:3 of maximum thrust and also thrust vector control.

For the design and optimization of the HRE the DLR software tool AHRES is applied. Within this paper, results of interior ballistic computations, heat transfer and temperature distribution inside the combustion chamber, as well as the properties of pressure feed system are shown and analyzed. The solid fuel grain geometry is designed using the burn-back module STAR (part of DLR AHRES software tool), which is coupled with optimizer NOMAD (based on direct search optimization algorithm). For the moveable nozzle with ablation, gas flow properties, temperature distribution within multilayer structure, radial and tangential stresses as well as structure dilatations for each CAD plane in longitudinal axis direction are presented.

Keywords: Hybrid rocket engine, upper stage, AHREUS, interior ballistic, design, mass analysis, HTP

ABBREVIATIONS

AHRES	Advanced Hybrid Rocket Engine Simulation	EMA	Electro Mechanical Actuator
AHREUS	Advanced Hybrid Rocket Engine Upper Stage	FEM	Finite Element Method
CAD	Computer Aided Design	GAP	Glycidyl Azido Polymer
CFD	Computer Fluid Dynamics	H_2O_2	Hydrogen peroxide
CMC	Ceramic Matrix Composite	O/F	Mixture ratio oxidizer/fuel
DLR - AS	DLR Institute of Aerodynamics and Flow Technology	HRE	Hybrid Rocket Engine
		HTPB	Hydroxyl-terminated Polybutadiene
		HTP	High Test Peroxide (H_2O_2)
		LRE	Liquid rocket engine

NTO	Nitrogen Tetroxide N_2O_4
PE	Polyethylene
PEG	Polyethylene Glycol
PUR	Polyurethane
VLM	Veículo Lançador de Microsatélites
VSM	Vehicle Service Module
RCS	Reaction Control System
SRE	Solid Rocket Engine
SHAKIRA	Simulation of High Test Peroxide Advanced Catalytic Ignition System for Rocket Application
TVC	Thrust Vector Control

SYMBOLS (LATIN)

A_e	m^2	Exit area of the nozzle
A_t	m^2	Throat area of the nozzle
c*	m/s	Characteristic velocity
c_p	kJ/kg	Heat capacity (p = const.)
F	N	Thrust
I_{sp}	m/s	Specific impulse
$I_{sp,vol}$	kg/s m^2	Density impulse
I_{tot}	Ns	Total impulse
v, w	m/s	velocity
T	K	Temperature

SYMBOLS (GREEK)

ε	-	A_e/A_t – area ratio
ρ	kg/m^3	Density
γ	-	Heat capacity ratio c_p/c_v
η_{C*}	-	Combustion efficiency
η_{CF}	-	Nozzle efficiency
η_{Isp}	-	Overall engine efficiency
O/F	-	Mixing ratio

I. INTRODUCTION

The motivation for this technical analysis was the enquiry of DLR MORABA – Oberpfaffenhofen in Munich to the DLR Institute of Aerodynamics and Flow Technology, Dept. Spacecraft (AS-RFZ), to recommend the solution for a new more efficient upper stage for the VLM launcher (in version for orbital application).. The goal was to show that a hybrid rocket engine (HRE), designed for an upper stage, is one suitable solution for the 3rd stage propulsion of the VLM launcher. This solution shall have more new features such as multi-ignition, thrust throttling and thrust vector control. Furthermore, the allowed engine volume inside the vehicle fairing and engine weight shall not be higher than for the currently chosen solid rocket engine.

The predesigned engine under the code identifier AHREUS (Advanced Hybrid Rocket Engine Upper Stage) is realised with the CAD system CATIA V5. The necessary calculations for the engine design were accomplished by using the Advanced Hybrid Rocket Engine Simulations (AHRES) software tool developed by AS-RFZ Braunschweig. Nearly all parts of the designed engine can be produced with currently available technology. Additional experiments/studies are only necessary for the evaluation of an advanced catalyst pack, the thrust control system and some technologies used for bonding metal and CFRP structures. Additionally, the fuel regression rate properties of some perspective binder mixtures and metal ingredients have to be tested.

II. STATE OF ART BY HRE R&D AS A BASIS FOR AHREUS DESIGN

II.I. HRE Features and drawbacks

Advantages of HREs like safety, reliability, operating flexibility, simplicity, low development, recurring costs and low environmental impact are well known and discussed in many papers [1, 2, 3, 12, 13, 14]. Therefore, they are not elaborated in the present report. The classic HREs also possess some drawbacks as drifting of O/F-ratio from the desired value, slightly lower combustion efficiency compared to solid and liquid propulsion systems, lower grade of combustion due to sliver, lower regression rate of solid fuel grain (consequence is a low thrust level) and finally the higher dry mass compared to solid engines (higher construction mass). The latter can be neglected, if the achievable specific impulse of HRE is so much higher that the difference of I_{sp} to the solid rocket engine (SRE) can compensate the differences in dry mass (usually 15% to 40% dependent on propellant type and combustor design). In other words, the density impulse $I_{sp,vol} = \rho\, I_{sp}$ must exceed the one of the SRE and it has to be comparable with liquid storable rocket engines. In this case, the HRE will have a chance for practical applications.

II.II. Current emphasis by DLR research within AHRES Program

In 2008 the Institute of Aerodynamic and Flow Technology of DLR started activities to investigate HREs how the latest technology achievements in the area of CFD modelling, light weight and high temperature structures, combustion control and optimised feeding/injection of the liquid propellant component can be used to design a highly efficient, safe and environmental friendly HRE. For this purpose the DLR test facility Trauen has the possibility to test hybrid rocket engines up to 10 kN. The test program is currently restricted to the application of storable high test peroxide (HTP) with H_2O_2 concentrations equal or higher than 87.5 wt% (oxidizer) and polymer fuels with or without metal additives [4, 7, 9, 10, 11, 18]. Currently, ten tests were carried out successfully. The results indicate

that an efficient HRE for space application is feasible. The application of new materials (CMC, CFRP, phenol based ablators etc.), new propellant formulations, new sophisticated computer tools (CAD, CFD, FEM) and common control technologies, obviously enables to eliminate most of the drawbacks of HREs.

The designed and tested AHRES hybrid rocket engine consists of a catalyst chamber with subsequent combustion chamber (Fig. 1). As oxidizer the 87.5 wt% hydrogen peroxide is used, which is decomposed by silver meshes inside of the catalyst chamber to water steam and oxygen at 650 °C.? The catalyst chamber can be operated on its own and it is capable to decompose up to 1.5 kg/s of H_2O_2. Tests have shown that the catalyst temperature has to be 300 °C or higher before a high mass flow can be decomposed, but pressure oscillations will be much lower, when the final temperature of the catalyst is reached[5]. The preheating of the catalyst is carried out with a small mass flow of hydrogen peroxide.

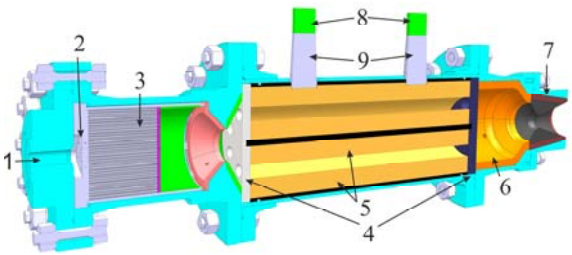

Fig. 1: AHRES hybrid rocket engine: 1-oxidizer inlet; 2-injector head; 3-silver mesh; 4-vortex plates; 5-fuel; 6-heat shield; 7-graphite nozzle; 8-ultra-sonic transducer; 9-delay line.

The solid fuel grain geometry is a telescope configuration, with an inner rod of 55 mm and an outer tube of 90 mm inner, and 140 mm outer diameter. The overall grain length is 376 mm. The baseline solid fuel is HTPB and ingredients like aluminium, magnesium-aluminium alloy, magnesium hydride and carbon powder are examined. To determine the regression rate of hybrid rocket solid fuel under different oxidizer/fuel-ratios and different additives an ultrasonic system is used. The combustion chamber is equipped with two measurement points for the regression rate which are positioned in row. The system is operated at 100 Hz ultrasonic pulse repetition rate, while the return signal is recorded at 100 MHz. Several potential sources of errors due to the chamber pressure fluctuations and temperature profile affect the ultrasonic measurement and must be considered. Therefore the results of the time-related ultrasonic measurement are verified with a caliper measurement before and after the test run. A detailed description of the ultrasonic system is given in reference[6].

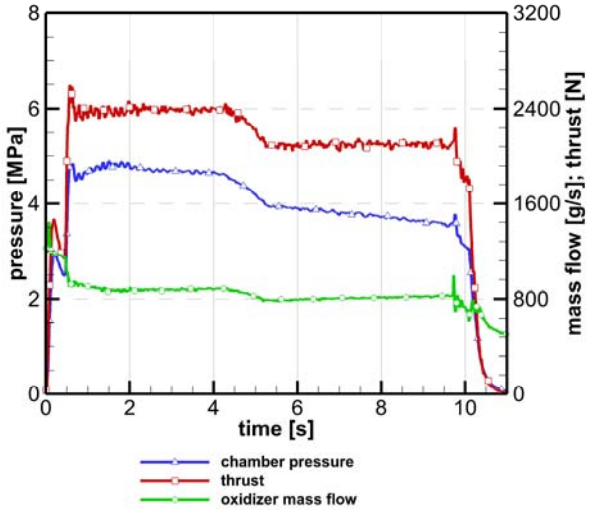

Fig. 2: AHRES test run number 4.

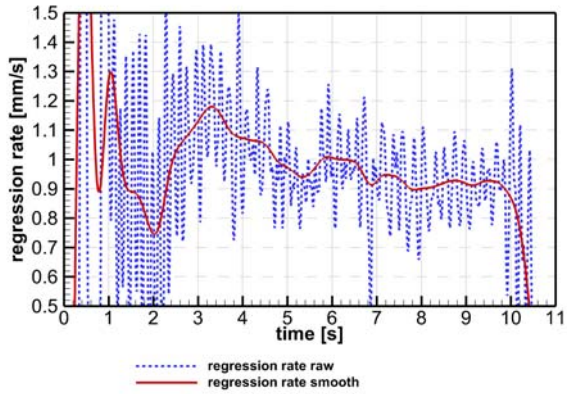

Fig. 3: Ultrasonic regression rate measurement.

In 2013 and 2014 ten hybrid rocket tests with HTP oxidizer were carried out. The applied solid fuels were 4 times pure HTPB and 6 times HTPB with aluminium powder. In Fig. 2 example data of an aluminium test is given. A mean chamber pressure of 4.5 MPa was used and the engine achieved a thrust of 2400 N. During second 4 and 5 the oxidizer was throttled for about 10%, as a consequence, the regression rate is falling from about 1.1 mm/s to nearly 0.95 mm/s. This effect can be seen in the ultrasonic regression rate data in Fig. 3.

Another experimental apparatus for measurement of regression rate and investigation of combustion processes is going to be operational at beginning of the year 2015, a rectangular combustion chamber with side windows to observe the flow field above the fuel specimen. Through the windows, the boundary layer structure can be measured and recorded. The fuel specimens are 18 mm thick, 50 mm wide and 350 mm long. To decompose the hydrogen peroxide, the same

catalyst chamber is used as for the AHRES hybrid rocket engine.

Fig. 4: Labor arrangement for characterization of combustion process at the boundary layer near the reacting surface of fuel specimen.

Apart from a number of points for thermocouples inside the fuel specimen also the two ultrasonic sensors can be applied at the rectangular chamber. The chamber is designed to operate at up to 2.5 MPa pressure. It is very difficult to build an experimental combustion chamber with glass windows that is suitable for operation with pressures up to 70 bar with currently available off-the-shelf materials. This pressure range corresponds to values, which are to expect for HRE in aerospace applications. For very low operation pressures and mass flows the combustion process is predominantly controlled by diffusion. For pressures higher than 2.5 MPa one expects more influence of the reaction kinetics on the combustion process.

The experimental work is completed with theoretical investigation of the combustion process inside of HRE. The AHRES design tool is validated through the own HRE experiments carried out on the at DLR test range Trauen. Additionally to the AHRES design tool the DLR Navier-Stokes code TAU which enables also the simulation of reaction kinetics and heat transfer within a combustion chamber flow.

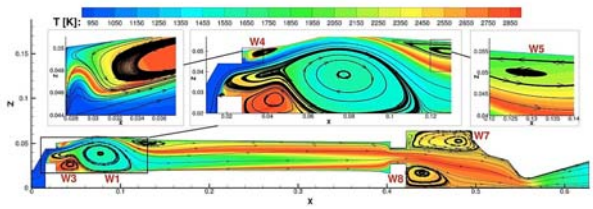

Fig. 5: Temperature distribution and streamline evolution of the 2D simulation at the point in burning time 10 s after the ignition of the AHRES engine (CFD simulation –Stefan May [10, 17]).

The TAU code, once validated for HRE's by well-defined experiments, enables the prediction of a large number of working regimes inside the HRE combustion chamber and the improvement of its geometry. An example of a numerical analysis is given in Fig 5.

III. DESCRIPTION OF THE AHREUS UPPER STAGE

Fig. 6 displays the cross-section of the predesigned HRE upper stage for the VLM-1 launcher. The displayed engine consists of the following main subsystems:

- high pressure gas feeding system,
- the oxidizer tank for the liquid 98 wt% HTP,
- a gas generator, based on the HTP catalyst chamber with multi-ignition capability,
- a ring-shaped injector head with swirl injectors for the decomposed gas mixture and liquid HTP,
- combustion chamber with an embedded solid fuel grain,
- mixing chamber (post-combustor)
- ablation cooled nozzle,
- control system for thrust throttling and engine condition monitoring,
- two-axis Thrust Vector Control (TVC) system with electro mechanical actuator (EMA),
- thermal protection for oxidizer tank and combustor.

AHREUS has a thrust level of approx. 31 kN. The designed gas pressure feeding system enables a better propellant to structure mass ratio, compared to a feeding system based on a turbo-pump. For the present case, such a concept is more simple, more reliable and cost effective. The feeding system consists of a toroid pressure tank made of carbon-fibre-reinforced plastic (CFRP) T800. The tank has an interior volume of 0.168 m^3 and accumulates up to 10.84 kg of helium gas at a pressure of 40.0 MPa. In the feed line, which connects the high pressure helium tank and the HTP oxidizer tank, two electrically controlled solenoid valves are incorporated. They hold the output gas pressure at 10.0 MPa. The oxidizer tank, which is also of toroidal shape to reduce the overall engine length, has a capacity of 0.440 m^3 for the 98 wt% HTP. The basic oxidizer tank structure is made of 3D braided CFRP T800 material coated with PTFE on the interior wall side. Four pipe lines for feeding the oxidizer from the tank to the combustion chamber lead into a collector which houses the two-stage regulator valve. The regulator valve distributes approx. 58% of the oxidizer mass flow (primary flow) into the catalyst chamber and the rest of the total oxidizer mass flow (approx. 42% at nominal thrust load) to 6 swirl injectors for liquid HTP[8]. A manifold integrated in the combustor head distributes the liquid oxidizer flow to the radially distributed swirl injectors. In the catalyst chamber, the liquid HTP flow

evaporates and catalytically decomposes to gas mixture of oxygen and preheated water steam. At the exit of the catalyst chamber this gas mixture has a temperature of approx. 1000 °C. This ensures that this primary gas flow and the fine spray from the swirl injectors have a sufficient temperature to ignite the solid fuel after mixing. This multi-phase oxidizer flow forms itself close to combustor head of the HRE. The oxidizer injection described here enables the multi-ignition capability of the hybrid rocket engine.

The combustor has a cylindrical form and a simple structure, which enables an easy and cost-effective production. The combustor volume is divided in two

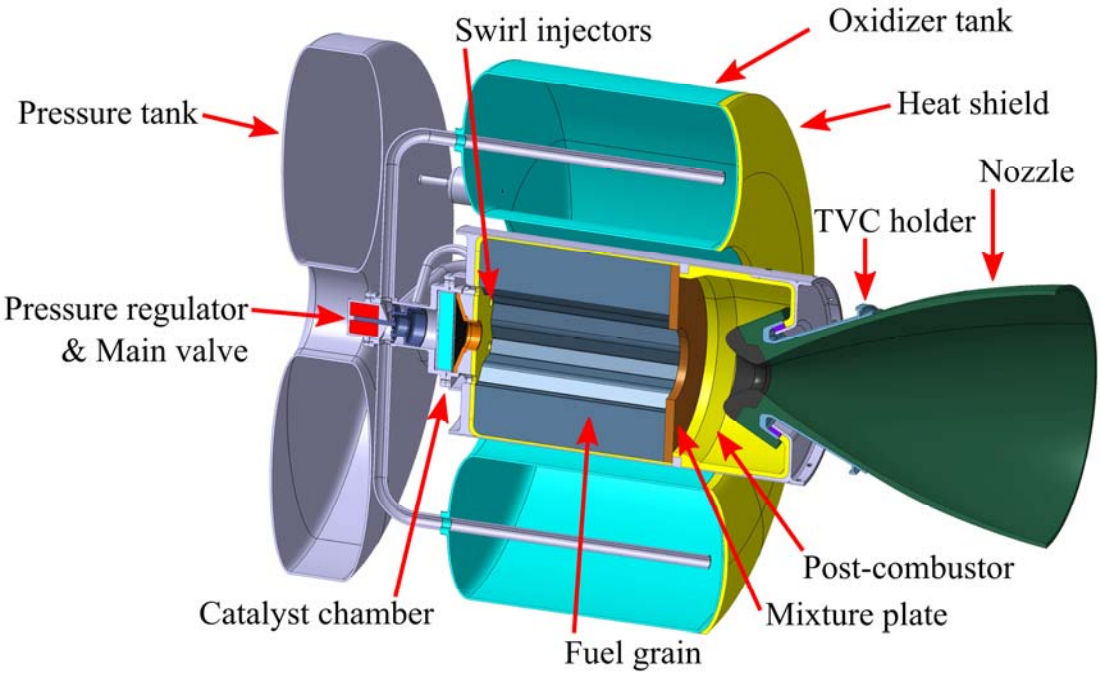

Fig. 6: Cross section of the AHREUS engine.

zones – gasifier and post-combustor, physically separated by a mixing plate (turbulence disc). The upper combustor part (gasifier) incorporates the solid fuel grain with an interior flow channel. The cross section of the flow channel is star shaped with 6 flat spikes.

This enables a moderately progressive thrust evolution of approx. 31 kN. In the calculations the change of the nozzle throat diameter due to erosion is not taken into account. The optimisation of fuel grain geometry with a star shape is realised using the coupled STAR module and NOMAD optimiser [9, 11]. After injection in the gasifier zone, the oxidizer has a gas temperature higher than 450 °C, sufficient to start the pyrolysis of the solid fuel grain. In the boundary layer, close to the reaction surfaces inside the interior channel, a thin flame front is established. In the flame front the mixture ratio O/F is approximately stoichiometric and the corresponding combustion temperature for the selected propellant mixture is approx. 2870 °C. But it is not assured that the whole oxidizer from the core stream will react with the products of the fuel pyrolysis. To enhance the probability of mixing and the complete reaction between oxidizer and fuel, a mixing plate is integrated in the chamber, which will additionally increase the turbulence of the reacting components. To increase the residence time of the reacting gases in the combustor and therefore, the combustion efficiency, an additional mixing chamber (post-combustor) is added upstream the moveable nozzle. To survive the severe thermal loads, the interior surfaces of the post-combustor are protected with a high density phenol based ablator, reinforced with carbon fibres.

To reduce the length of the motor, the nozzle is plunged into the combustion chamber. It consists of a fixed and a moveable part. The moveable part of the nozzle is controlled by two EMA as a part of TVC. The fixed part of the nozzle (nozzle holder) is designed as a truncated cone and is integrated to the combustion chamber casing. The moveable part is in fact a Laval nozzle with reduced subsonic contour, a robust nozzle throat and a large supersonic bell. These two parts of the nozzle are coupled using an elastic sandwich structure, which consists of laminated epoxy-glass-fiber disks and synthetic rubber layers (violet colored parts on Fig. 6).

This elastic structure allows turning the nozzle around the pitch and the yaw axis with an angle up to 6.5 degrees and acts as sealing ring as well. To fix the sealing ring on the high thermal loaded basic nozzle structure, two conical thin rings are attached (dark grey colored parts in Fig. 6). These rings are made of stainless steel 1.4841.

The supporting base structure of the fixed nozzle part (shaped as truncated cone) and moveable nozzle parts of the nozzle (bell shaped) is made of AlSi7Mg0.6 (glow grey colored parts in Fig 6). The supporting structure of the fixed part is protected from high thermal loads using the phenol ablator, reinforced with carbon fibers (developed by INVENT Co., Braunschweig). For the thermal protection of the supporting structure of the moveable nozzle part, carbon-carbon composite material (e.g. SEPCARB – pyrocarbon + pitch coke) and ablative composite materials are used. The inner subsonic and supersonic parts of the nozzle are exposed to high thermal and erosion loads, but the erosion loads are lower than in the nozzle throat. For that reason, they are coated with ablative material of the types MX-4926. This material is composed of phenolic resin and 2D plaited carbon fiber. The nozzle throat is exposed to the highest thermal loads, erosion and hot gases, and it is protected with a C-C composite structure (e.g. NOVOLTEX).

IV. SELECTION OF HRE PROPELLANT MIXTURE

In the frame if this work thermochemical properties of various fuel mixtures combined with hydrogen peroxide (HTP) of different grades as oxidizer are reviewed. Following fuels were considered: Polybutadiene (HTPB), paraffin, polyethylene (PE), Polyurethane (PUR), Polyethylene Glycol (PEG) and Glycidyl Azido Polymer (GAP). Also the influence of diverse metal ingredients (additives) on heterogeneous propellant properties is analyzed. Especially the influence of the mass fraction, of the single component, on the energetic properties of flammable mixture (e.g. specific and volume impulse, characteristic velocity), engine controlling (O/F mix ratio) and physical-chemical properties of fuel grain is considered. In the focus was also the influence of these properties on production technology and mechanical stability of fuel grains. In the analysis the minimum mass fraction of HTPB binder is limited on 42 wt%, to prevent the problem with mechanical stability of grain and bonding capability of other additives. Furthermore, to provoke the increase of regression rate also is considered application of miscellaneous binder mixtures, but in attendance of metal ingredients.

Fig. 7 shows the change of specific impulse as a function of O/F mixture ratio due to the influence of various polymer binders (subordinate binders) added to HTPB. The mass fraction of subordinate binders (paraffin, PE, PUR, PEG, GAP) is retained on 20 wt% of the fuel mixture. The content of HTPB is for all calculated cases kept at 50 wt%. The additionally applied metal ingredient -magnalium (name of commercial product) with mass fraction of 30% is an alloy of magnesium and aluminum. As oxidizer HTP (mass fraction of H_2O_2 is 98 wt%) is applied. The results of the calculations carried out with CEA2 code[16] indicate that the pure HTPB (100% of fuel) has a maximum I_{sp} of 3222 m/s at a O/F mixture ratio of 6.8. Through the add-on of 30 wt% aluminum in the HTPB (70 wt%) the specific impulse increases only by 1.6% to 3274 m/s and O/F maximum mixture ratio reduces to 4.9 (less suitable for thrust throttling control).

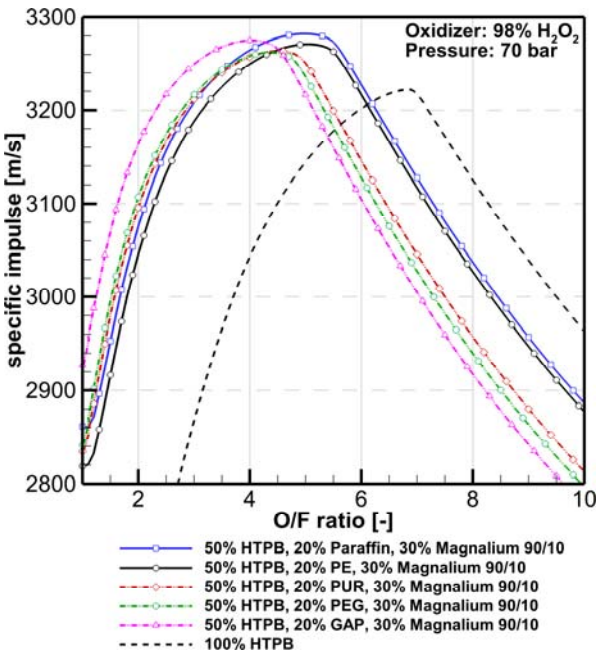

Fig. 7: Specific impulse versus O/F-ratio by application of diverse subordinate fuel binders and metal ingredients.

If the aluminum is exchanged with magnesium the I_{sp} reduces but is still higher than for pure HTPB. The application of metal ingredients makes only sense if the hybrid engine compactness or an increase of regression rate can be achieved. One interesting high energy fuel formulation for current applications, which shall be

further experimentally investigated, is magnalium with high aluminum content in alloy (I_{sp} is approx. 3270 m/s). The insertion of paraffin and GAP in the fuel mixture can theoretically slightly increase the I_{sp} for 5 to 11 m/s, but brings technological or security problems. Paraffin is desired as subordinate binder, because it significantly increases the regression rate. But tests carried out by DLR-AS Braunschweig show that such mixture has much lower mechanical properties than HTPB. Mixtures of PUR and PEG with HTPB are possible, but they have slightly lower I_{sp} than favorable HTPB/PE-mixture and also the optimum O/F mixture ratio is with value 4.5 more unfavorable with respect of thrust throttling capability. GAP is classified as explosive matter and despite its high I_{sp} this would be an important disadvantages to HRE if applied. These drawbacks have consequences on simple production, storage, transport and handling regarding the costs. With respect to the upper examined relevant criterions, the fuel mixture of HTPB/PE/ magnalium shows the highest potential for short term application. It is valid under the assumption that a very high regression rate is not required.

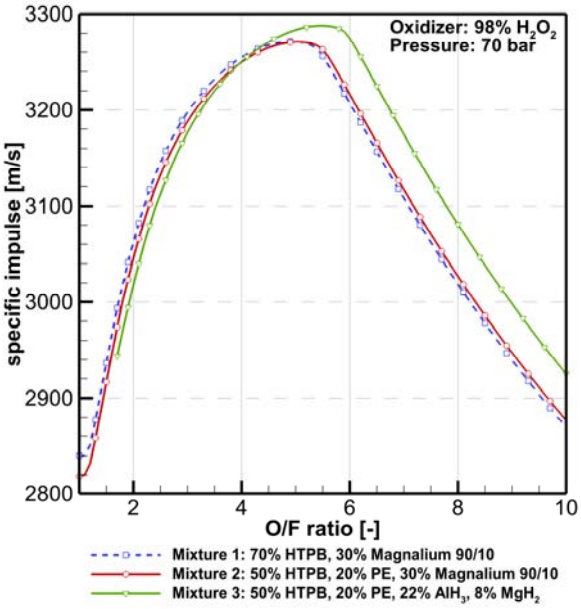

Fig. 8: Specific impulse versus O/F-ration for selected propellant mixtures.

In the next selection loop the weight percent of polyethylene and magnalium content in the fuel mixture is varied (s. Fig. 8). The HTPB content in this mixture model [19, 20] was fixed on 50 wt%. The best compromise between energetic, physical and technological properties show the composition of 50% HTPB/20% PE/30% magnalium (mixture 2 in table 1). The corresponding regression rate is estimated on the basis of Chiaverini's theoretical laws[19,20]. For further details see the Chapter V.III. One further comparison between the favored HTPB-PE-Al/Mg fuel mixture and other for application interesting mixtures is done applying mixtures of metal hydrides (alane ALH_3 and magnesium hydride MgH_2 – s. the mixture 3 in table 1) instead of magnalium. One reasonable content of metal hydrides in the fuel mixture between 30 and 38 wt% deliver the I_{sp} gain of only 0.6 to 1.2% compared to reference fuel mixture 2 and slightly shift of optimal O/F mixture ratio from 5.0 to 5.5.

Propellant mixture	**1**	**2**	**3**
Density [kg/m^3]	1138.8	1144.8	1041.6
Specific impulse [m/s]	3271.6	3271	3288
O/F ratio	4.9	5.0	5.5
Chamber temperature [K]	3167.1	3152.6	3106.0
Heat capacity ratio $\gamma=c_p/c_v$*	1.1961	1.1977	1.2044

*ratio of exhaust gases

Table 1: Analyzed propellant mixtures of the AHREUS predesign loop.

The fuel composition based on metal hydrides with a density of 1041.6 kg/m^3 has noticeably lower density impulse $I_{sp,vol} = \rho\, I_{sp}$ [kg/m^2 s] than the reference mixture 2. Thus the construction mass of the combustion chamber must increase too and the resulting recalculated "gain" of I_{sp} is rather negative. The main advantage of fuel mixtures with metal hydride content could be an increase of the regression rate[18]. Further tests on the HREs demonstrators are necessary to assess the potential for practical application in aerospace of this fuel composition. For short term applications, the number of unknown consequences by combustion and core flow, together with high acquisition costs and poor availability, exclude the fuel compositions based on metal hydrides as design solutions.

V. DESIGN OF MOST IMPORTANT AHREUS COMPONENTS

V.I. Pressure feeding

The general description of the feeding system is summarized in chapter 3. For presented feeding system the hydraulic and pneumatic resistances inside the regulating valves, feeding lines, catalytic chamber, gas

swirl injectors and combustion chamber head which include a set of liquid swirl injectors are calculated. The central feeding line, coming from the oxidizer tank, is divided into two branches downstream the control valve. The first branch leads over the catalyst chamber (blue dash line, Fig. 9) and the second over the head manifold and liquid injectors (red full line). The total pressure difference between gas pressure tank and combustion chamber, calculated under steady conditions, is 30 bar. The described pressure cascade appearing within the feeding system is displayed in Fig 9. Currently the dynamic properties of hydraulic system are analyzed.

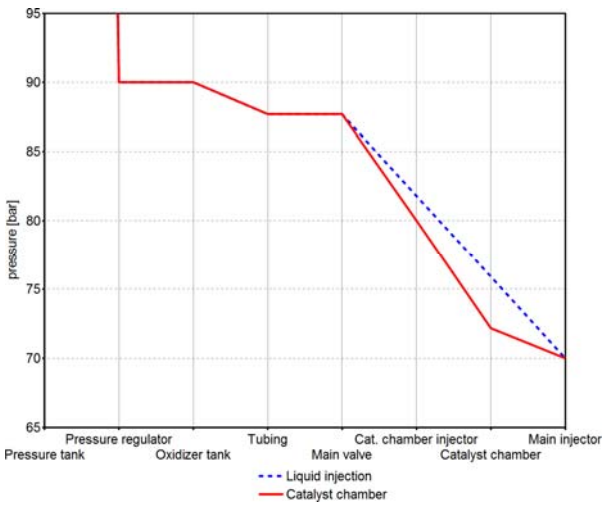

Fig. 9: Pressure cascade devolution within the feeding system.

V.II. Catalyst chamber

If a HRE with HTP oxidizer is equipped with catalyst chamber, the process in the main combustion chamber can be organized more efficient. The ignition system can be very simple or completely eliminated. If the entire oxidizer mass flow streams through the catalyst chamber, the injection of liquid HTP and its atomization into droplets respectively evaporation can be omitted. In the catalyst chamber the HTP decompose to pure oxygen and water steam (overheated).

The decomposition of 98 wt% HTP results in an adiabatic temperature of 1282.15 K and corresponding species mass fraction is 46 wt% O_2 and 54 wt% H_2O steam. But for this design case the construction mass of catalyst chamber is not acceptable, especially for engines with higher thrust level. To use the important features of catalyst chamber, despite declared disadvantage, a tradeoff has to be found. It seems that the compromise solution is the use of liquid HTP injectors and a catalyst chamber on the combustor entrance. If the mixing temperature of the primary (through catalyst chamber) and secondary (through liquid injectors) oxidizer mass flow is fixed to 450 °C (723.15 K) the individual mass flow through liquid injectors and catalyst chamber can be estimated using the mass and energy balance of the oxidizer. As a result for 98% HTP the mass flow through catalyst chamber should be lower than 57% of total oxidizer mass flow. Such catalyst chamber can be short and efficient, which is beneficial for the HRE construction mass ratio. For the design of the catalyst chamber the software module SHAKIRA is used. It enables the construction, and the calculation of flow properties and heat loads for different types of catalyst beds.

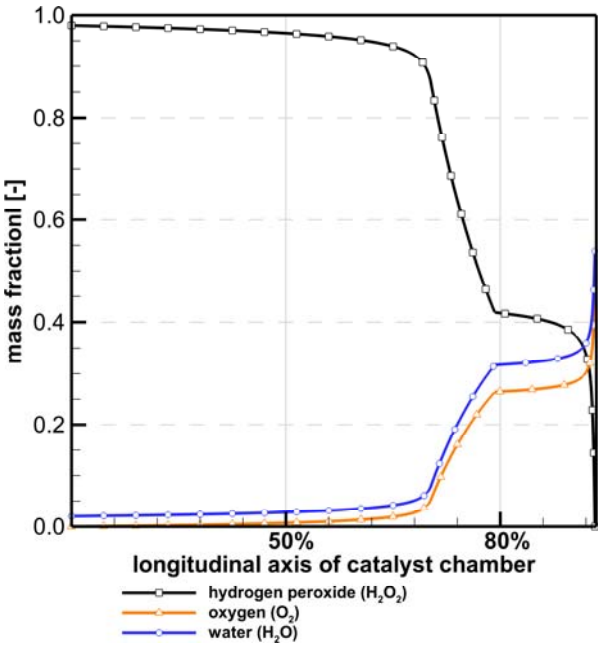

Fig. 10: Fraction of the hydrogen peroxide, oxygen and water steam along the length axis of catalyst chamber.

Results of calculation, carried out for pebble bed geometry with platinum coating on aluminum oxide buffer are shown in Fig. 10. At the beginning of the catalyst chamber the decomposition of 98 wt% HTP (liquid mixture of pure HTP and 2 wt% water) is low and the fluid temperature rise slowly. At ca. 70% of total chamber length the temperature of gas/steam mixture reaches a peak of 415 K and then the HTP decompose rapidly. Synchronously the mass fractions of O_2 and H_2O steam rise exponentially and achieve their maximum value at the chamber exit plane.

V.III. Solid fuel grain

The requirements for AHREUS engine is that it shall deliver an average thrust of approx. 31 kN, constantly available for the entire burning time. This requirement can only be realized with a telescope (cylinder in hollow cylinder) or a star shaped fuel grain (s. Fig. 11). The application of telescope fuel grain form is connected with the problem of safe attachment of interior cylinder to the structure of combustion chamber and simultaneously undisturbed flow of combustibles gases. The high temperature, the high heat transfer flux and erosion effects (especially by attendance of combustibles gases) make the attachment of this fuel grain the very difficult construction problem. This problem appears already after burn times over 30 s.

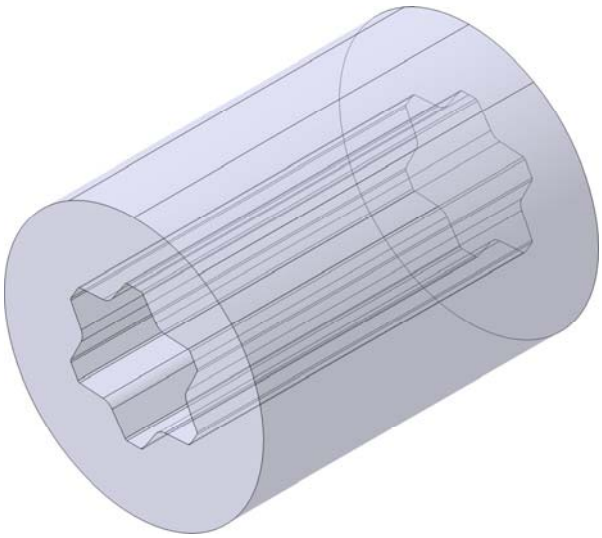

Fig. 11: Designed fuel grain with star shape (result of an optimization).

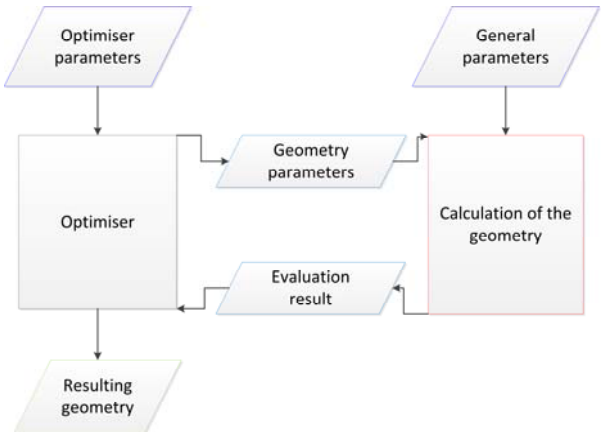

Fig. 12: Workflow for the optimization of the fuel grain.

The star geometry form offers a more simple and effective solution. That was the reason to select a star geometry for AHREUS engine. But to find the corresponding star geometry form with neutral (approx. constant) thrust profile is not a simple task, because a number of star design parameters which fulfill this condition must be found. Due to the complexity of this task an optimizing tool is used, which sampled the different design parameters and on the basis of the weighting function revised its selection. The in-house developed burn-back program for star grain form shaped fuel blocks was coupled with the optimizer NOMAD (Non-linear Optimization by Mesh Adaptive Direct Search).

In doing so, a multidimensional grid of variables is stretched (in case of the star grain shape 8-dimensional)[23]. The workflow of the optimizing method is given on Fig. 12.

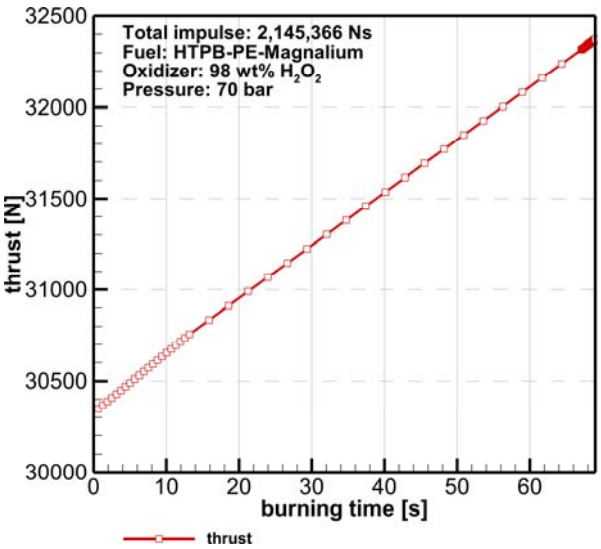

Fig. 13: Thrust run for the optimized fuel grain with star shape.

For propellant mixture 2 and given input data for star shape (s. Tab. 1) after 1400 iteration steps the prescribed accuracy limit of NOMAD optimizer was achieved. The result of optimizing procedure is a fuel block shape with a diameter of 0.45 m and a length of 0.573 m. The interior flow channel has a star shape with 6 spikes and fuel fill factor of 78.2%. The sliver loss of fuel is calculated on 0.7%, which is very low. The isometric view of fuel block is presented in Fig. 11. At the end of the first optimization loop the prescribed values total impulse of the engine and the corresponding thrust are obtained.

VI. INTERIOR BALLISTICS

To characterise the interior ballistic process the distribution of local flow pressure p, total flow pressure p_{tot}, hot gas temperature T, hot gas velocity v and gas density ρ within the interior flow channel of the propellant are determined. The distribution of above specified characteristic flow values along of the longitudinal x-axis of the SRE is determined using the Raizberg-Erohin-Samsonov-Method (RESM) [15]. This method takes the non-uniform velocity distribution in the interior channel into account. It is caused by friction and heat transfer from hot gases to the reacting channel walls. RESM is valid under the following assumptions:

- the flow is quasi-steady, 2D axis-symmetric and viscous,
- the flow is viscous, incompressible and without vortices,
- the channel walls are porous for combustible hot gases,
- the hot gas flow does not contain condensed phases (droplet or solid particles).

The RESM can be integrated to deliver a system of analytic functions, which describe the aforementioned characteristic values of the interior channel flow. In basic form the results are valid for a cylindrical channel. For arbitrary channel shape (star, finocyl e.g.) the hydraulic radius, defined over the wet flow perimeter and the free cross-section area, for hot gas flow can be taken as radius. To define the characteristic flow values (p, p_{tot}, v, T, ρ) along the longitudinal axis, the whole channel with variable cross sections divided into 21 segments with different hydraulic radiuses. For the whole channel the computation is performed iteratively, calculating the characteristic flow values from segment to segment. This calculation method enables the simple and fast estimation of the flow properties during the burn of a star shaped fuel block (quasi-steady). The results of calculations are shown in the Fig. 14 to Fig. 17. For convenience the data are not displayed for all time steps. Additionally, the three important characteristic burn phases are numbered.

Generally, the level of regression rate is dependent on the numerous properties of the fuel and the combustionprocess and not simple to determine. In the frame of this work a modified regression model of Chiaverini [19] is applied. Within the DLR AS experimental work this model is tested[4] for the HRE propellant mixture HTP/HTPB-Aluminum.

The results in Fig. 14 show the distribution of the fuel regression rate for the hot gas flow. The calculated average regression rate integrated along the longitudinal grain axis and over the burn-out time delivers the value of 1.6 mm/sec. This regression rate is achievable with present technology without the necessity to use exotic HRE propellant mixtures. Fig. 14 shows that regression rate decreases over the fuel length as well as with increasing burning time. The decrease with the chamber length can be explained by the weakening of swirling flow generated in oxidizer injection area and through the increase of the boundary layer depth close to the reacting fuel surface. Due to the increasing of boundary layer thickness, the distance of flame front related to fuel surfaces under pyrolysis increased too and therefore, the heat transfer to these surfaces reduces. With progressing burning time the regression rate decreases due to the increasing hydraulic diameter of interior channel. This reduces the specific mass flow in the channel and as consequence the regression rate.

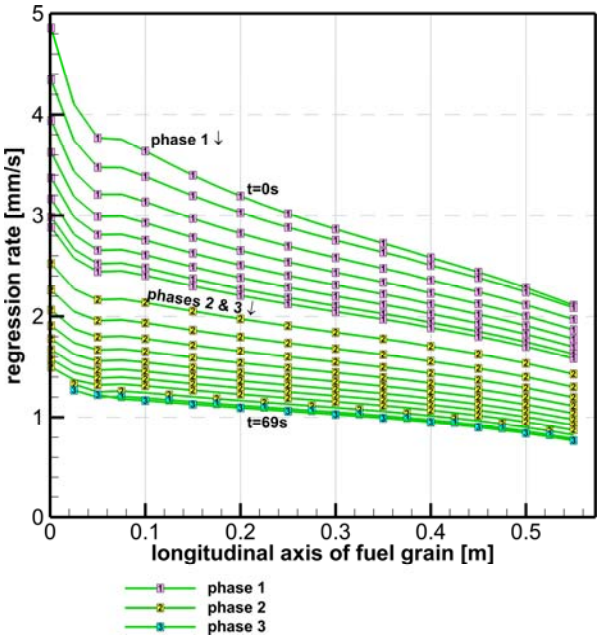

Fig. 14: Regression rate along the longitudinal axis of fuel grain channel at different time steps.

Fig. 15 shows the working pressure along the length of the combustion chamber for different time steps between start and burn out. The reduction of the pressure occurs due to flow friction in the boundary layer close to the fuel block surfaces.

The corresponding friction and heat transfer on interior surfaces of the fuel block is small, so the medium pressure loss of 3.5 to 12.6 mbar is negligible. Due to the

regression the diameter of inner channel of fuel block grows with progressing burning time. That also affects the friction and heat transfer. Over the burning time the pressure slightly increases (dependent on the designed star shaped fuel block) and the corresponding thrust also increases but only by 0.76% (s. Fig. 15).

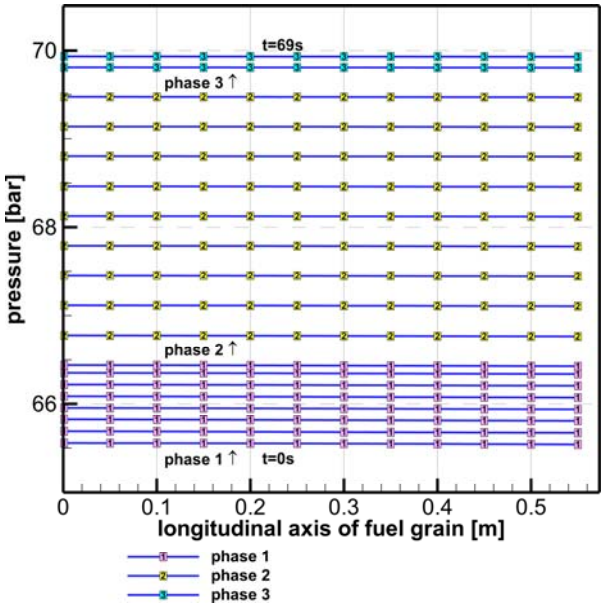

Fig. 15: Working pressure along the longitudinal axes of fuel grain channel for different time steps during burn out.

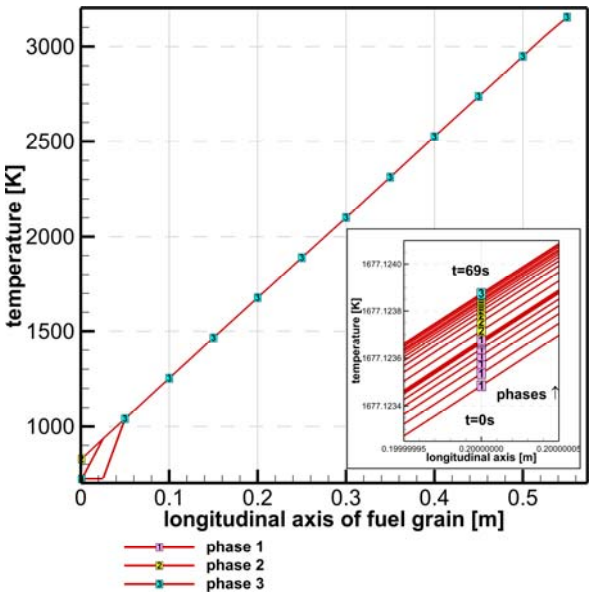

Fig. 16: Average temperature distribution along the fuel grain interior channel.

Fig. 16 shows the average temperature distribution of hot gas flow along the fuel gran channel. The temperature increases along combustion chamber (from injector side to nozzle). The start temperature is only slightly higher than the temperature of the injected oxidizer mixture, because the combustion temperature over the first intersection segment of fuel grain is taken into account.
In all further segments the continuously reducing oxidizer mass flow is mixed with growing mass of hot combustion products generated in the boundary layer. So, the average gas temperature increases in direction downstream direction. The flow is almost adiabatic because the fuel grain with predominantly polymer structure is a good isolator. So, the temperature development of the gas mixture is for different time steps nearly identical. The difference is inside 0.005 K. At the end of combustion process at the distance of the first 22 mm from injectors the fuel is already exhausted, so the gas temperature is equal the temperature of injected oxidizer.

The axial velocity distribution (average value) of the inner hot gas flow is shown in Fig. 17.

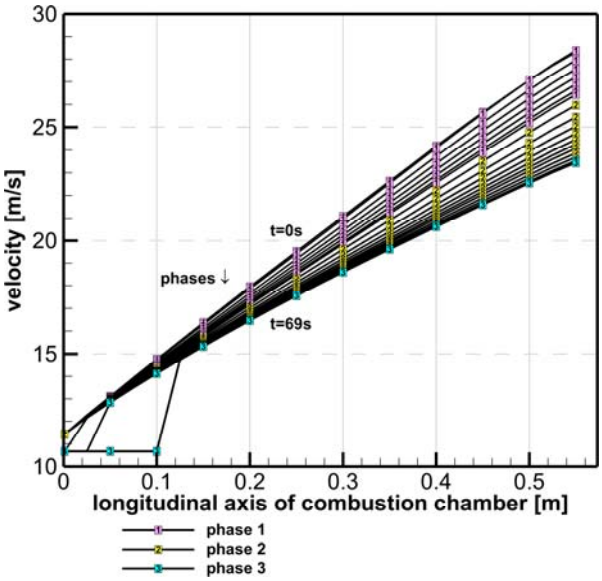

Fig. 17: Distribution of the average velocity along the longitudinal axis of fuel block as function of burning time.

In flow direction the velocity increases due to the mass flow increase of additionally pyrolysed fuel and combustion products generated within the reactive boundary layer. Causality, based on the conservation law (continuity equation), leads to a velocity increase. Additionally, the velocity increase is affected by the

increasing average flow temperature. In Fig. 17 it can be seen that the increase of velocity (gradient of the displayed curves) significantly decreases with progressing burning time. The hydraulic diameter of the flow channel increases and therefore the specific mass flow $\dot{m}/A_k$ reduces. Close to burn out the velocity on the first 22 mm of the channel remains constant. In this section the fuel is fully burnt down and the velocity determines only the oxidizer mass flow.

VII. NOZZLE PROPERTIES

The nozzle design properties are calculated with AHRES module DAPHNE-V2. For the designed nozzle (s. description of construction in Chapter III) the fluid properties are calculated (Fig. 18).

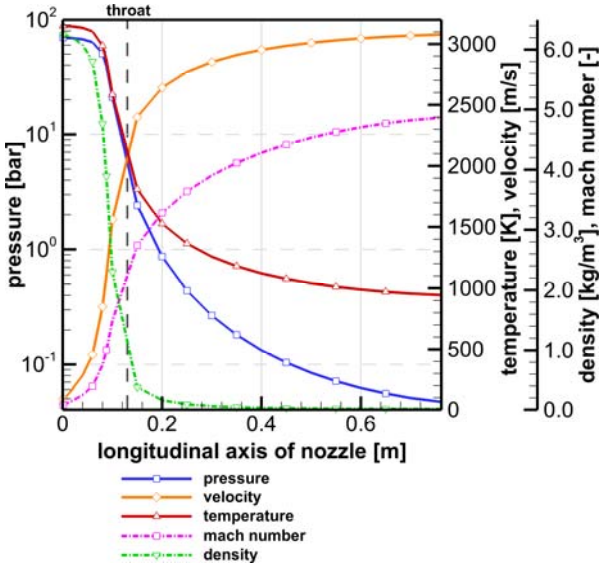

Fig. 18: Distribution of pressure p, temperature T_{gas}, density ρ and gas velocity w of the combustion products along the nozzle axis.

The flow is assumed as steady, isentropic and one dimensional; the combustion gases are simplified as ideal and homogeneous with invariant composition (frozen nozzle flow without chemical reactions). The heat transfer calculations are carried out under quasi-steady conditions. Thereby, the heat accumulation term was neglected.

The temperature distribution in the multi-layer nozzle structure with different materials in every cross section was calculated along the longitudinal axis of the nozzle (s. Fig. 19). The high temperatures at the wall surfaces in contact with hot combustion gases are partly a result of high Mach number effects. Based on increased friction effects at high flow velocities (especially in the supersonic part of nozzle), the gas temperature at the boundary layer T_{film} (violet curve) exceeds the average gas temperature of the nozzle T_g (red curve). The film temperature T_{film} (defined from Zielbland [21, 22]) is measured between the viscous sub-layer and the transition zone to the outer free turbulence zone. These three zones are part of the turbulent boundary layer along the nozzle contour. At high flow velocities, the film temperature affects also the nozzle wall temperature (s. Fig 18).

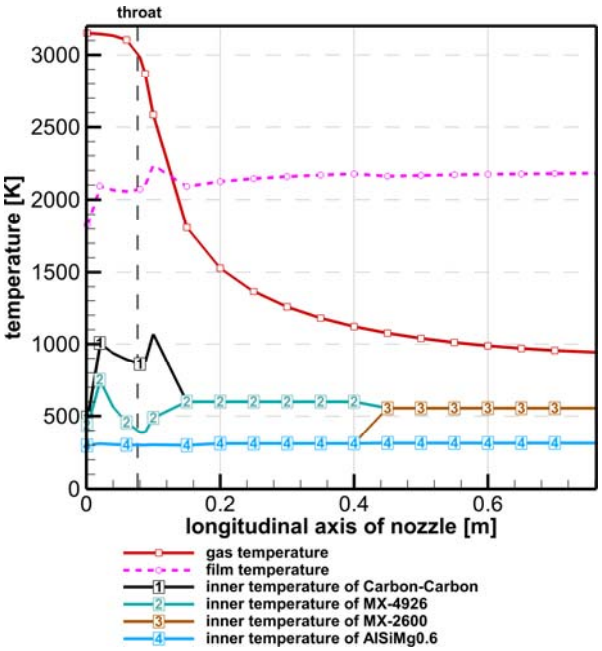

Fig. 19: Temperature distribution in the hot gas flow and inside the multi-layer structure along the nozzle axis (ablation taken into account).

By application of usual isolating material with passive thermal protection the calculated temperature values shall be very high, mostly above the limit of allowed material rigidity. The solution was to apply phenol based ablation material reinforced with carbon fibers (compare Chapter III).

In the AHREUS design case the ablation cooled nozzle is applied. At the contact surface between the pyrolysis zone and solid material, the temperature is always in the region of the lowest pyrolysis temperature of about 600 K. This temperature is used for the calculation of the heat flow to the engine's outer wall. Increasing gas temperatures and associated heat fluxes to the wall are compensated through the regression rate of the used ablative materials.

Therefore, the constructional safety of the nozzle is ensured. The ablation influence to the wall temperature is considered by the DAPHNE V2. For the case, that the temperature at the pyrolysis zone of the ablation layer stays under 600 K, what is confirmed by a number of calculations and experiments[7], the radial and tangential stresses at the internal and external walls of the nozzle remain under the yield strength of the used materials (s. Fig. 20).

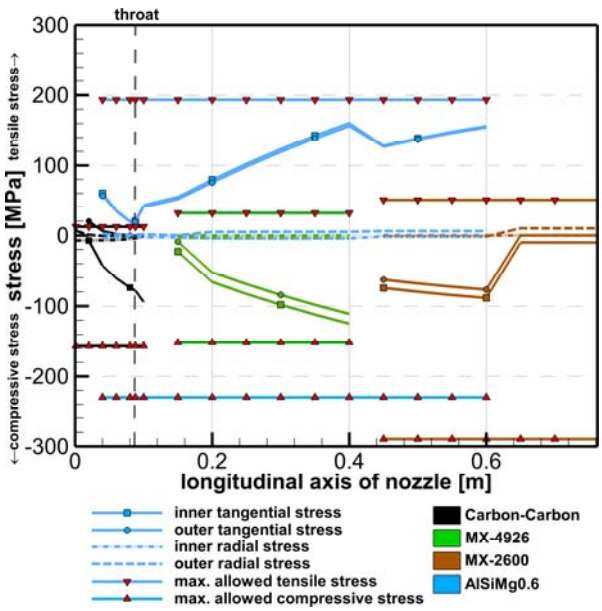

Fig 20: Distribution of the radial and tangential stresses at the inner and outer wall of the nozzle for each cross section along the x axis (ablation taken into account).

VIII. RESULT OF THE ENGINE COMPARISON

The comparison between the predesigned reference solid and the hybrid AHREUS is summarized in Table 2 and Table 3. The specific impulse of AHREUS engine is 9% higher than the one of the reference solid rocket engine. The coefficient of the specific impulse efficiency, which takes the combustion and nozzle efficiency into account, is estimated with realistic 92%. The coefficient of the specific impulse efficiency of the reference solid rocket engine, which takes into account the combustion efficiency and nozzle efficiency, is calculated to be 93%. To enable a fair comparison of the total impulse, the combustor design pressure and the burning time are assumed to be identical. As the thrust of both engines is comparable the calculation shows a higher mean mass flow for the solid rocket engine. This is the consequence of the lower specific impulse of this engine. With a high mean O/F mixture ratio for the selected propellant composition of 5.5 and a fairly flat I_{sp} = f(O/F) curve (s. Fig 8), the AHREUS engine is expected to be well suitable for thrust throttling capability. The test stand of DLR-AS enables an oxidizer flow modulation in a broad range. Recent tests with the AHRES engine demonstrated a thrust modulation between 800 and 2400 N with the same fuel geometry.

A CAD analysis carried out with CATIA V5 shows that, if the selected HRE propellant with a high density (over 1.15 kg/m^3) is applied, a compact form of the AHREUS engine can be achieved. In such a case, the AHREUS volume is comparable to the volume of the reference solid engine embedded inside the VLM launcher fairing. The selected solid engine has a diameter of only 1100 mm. To built-in the engine into the vehicle fairing (diameter 1.46 m) the implementation of an interstage adapter between 2nd and 3rd stage with an integrated bearer for the engine and an additional adapter to the Vehicle Service Module (VSM) is necessary. That leads to an increase of construction mass of the third VLM stage and makes the solid engine solution less effective.

With the outer diameter of 1200 mm, the AHREUS engine uses the available volume inside the 3rd stage casing more effective. Empty volume between the fairing (diameter 1.46 m) and the outer AHREUS diameter can be used to install an interstage hot gas RCS and a hot gas RCS for the VLM, both equipped with small monopropellant thrusters, based on 98 wt% HTP (vacuum specific impulse 1580 m/s). The mass balance, given for both propulsion systems in Table 2, shows that overall engine mass for the AHREUS engine (887.4 kg) compared to the reference solid engine (overall mass 990 kg) is for 102.6 kg lower. Taking the mass of the interstage RCS and the VSM cold gas RCS engines (based on nitrogen with specific impulse of 637.8 m/s) into account the mass gain of AHREUS thruster is still higher than 13%.

The construction mass of the hybrid rocket engine is, as expected, higher due to the additional mass of the high pressure helium tank, oxidizer HTP vessel and TVC/ thrust throttling system. But due to the higher specific impulse of the propellant, slightly higher expansion ratio of the nozzle and higher propellant density compared to alternative classic hybrid and liquid propellants, this construction mass drawback is successfully compensated.

Upper Stage Type		**3. stage Reference solid rocket engine + cold gas RCS**	**AHREUS advanced technology**
Parameter		**Value**	**Value**
Designer/ manufacturer		German industry	DLR – AS –RFZ BS
Propellant type		HTPB/NH_4ClO_4 /Al	98 wt% HTP/
Specific impulse – propellant $I_{sp,th}$	m/s	2813	3271
Vacuum specific impulse - engine	m/s	2616	3014.2
Total impulse	kNs	2145	2145
Medium vacuum thrust	kN	31.09	31.38
Overall combustion time	s	ca. 69	69 w/o throttling
Mean total flow rate	kg/s	11.88	9.42
Mean chamber pressure	MPa	7.0	6.93
Mean O/F mixture ratio	kg/kg	2.23	5.0
Mean regression rate (estimated)	mm/s	9.1	1.64 (range: 5.0 to 0.8)
Thrust modulation ratio	-	-	3.0
Nozzle expansion ratio **ε**	m^2/m^2	83	100
Number of re-ignitions	-	0	> 5
Construction weight (w/o propellant)	kg	160	179 + 18 (TVC)
Combustor casing	kg	-	26.63
Thermal insulation	kg	-	27.72
Nozzle incl. ablator	kg	-	28.7
Oxidizer tank	kg	-	40.68
Pressurisation tank with helium	kg	-	34.1
Catalyst chamber	kg	-	20.57
TVC: KW – 6,5°	kg	no TVC	18
Miscellaneous (reg. valves, pipe lines, start-stop valves e.g.)	kg	-	11.7
Oxidizer weight	kg	-	575.8
Solid Fuel weight	kg	-	115.2
Total propellant weight	kg	820	690.9
Igniter	kg	10	-
Start weight (col. 1: solid engine)	kg	990	887.4
Vehicle Service Module w/o RCS	kg	72	ca. 70
Interstage RCS	kg	22.5	12
VSM propulsion RCS	kg	43	28
Start weight 3. stage	kg	1127.5	997.4

Table 2: Comparison of the properties of the AHREUS upper stage concept and the reference solid rocket engine selected for the Brazilian VLM-1 Launcher.

Geometry	**[m]**	**[m]**
Upper Stage Type	**VLM 3. stage Reference solid rocket engine + cold air RCS**	**AHREUS advanced technology**
Diameter	0.6/1.080	1.200
Length - Upper stage incl. engine	1.510	1.625
Engine length incl. RCS for interstage and VSM	1.760	1.625
Nozzle throat diameter	0.066	0.055
Nozzle exit diameter	0.602	0.546
Nozzle length	0.744	0.737
Technical Readiness Level (NASA class.)	**7-8**	**5**
Cost factor	**1**	**1.5**

Table 3: Comparison of the dimensions of the AHREUS upper stage concept and the reference solid rocket engine for Brazilian VLM-1 Launcher.

IX. CONCLUSION

The discussed analysis shows that for the thrust level up to 50 kN the hybrid rocket engine (HRE) could be competitive to solid rocket engines. In the presented work it is shown that a HRE for upper stage application can be realised with common technologies and without the necessity to use exotic propellant combinations. The introduced AHREUS motor is compact and simple, which simplifies the production, montage, transport and the handling on the launch pad. The designed catalyst chamber for HTP decomposition and the pressure feeding system have a reasonably low mass and equipped with the advanced control system, based on common available technologies, it enables multi-ignition and thrust throttling. The introduced combustion chamber with moveable nozzle equipped with EMA enables also thrust vector control (TVC).

Based on the comparison, carried out for selected hybrid and solid upper stage engine concept, it can be concluded, that the AHREUS engine as an upper stage of the VLM launcher is superior compared to all aspects of the selected reference solid rocket engine (mass, energy efficiency, thrust vector control, ability of throttling and RCS manoeuvrability).

X. ACKNOWLEDGEMENT

The authors wish to acknowledge the contribution of Tobias Johannes Klaus, student of the Technische Universität Braunschweig, for the support by creating the CAD model of the AHREUS rocket engine. Also the authors thank M.Sc. Stefan May for permission to publish some results of the CFD simulation of the combustion process within the AHRES engine, realized within his master thesis. The authors are also grateful for the project support and helpful technical discussions of Dr. Thino Eggers, Head of Spacecraft Division DLR - AS Braunschweig.

XI. REFERENCES

[1] Božić, O., Porrmann, D. and Schneider, M., **Conceptual Design of "SILVER EAGLE" - combined Electromagnetic and Hybrid Rocket System for Suborbital Investigations**, 61st International Astronautical Congress (IAC), 27th Sept. – 1st Oct. 2010, C4.6. Special Session on "Missions Enabled by New Propulsion Technologies and Systems", IAC-10-C6.4.1, Prague, Czech Republic

[2] Orlandi, O., Blanschard, H., Yvart, P., Gautier, P., Galfetti, L., Paravan, C., Merotto, L., Boiocchi, M., Mazzeti, A., Maggi, F., DelLuca, L., Russo Sorge, A. and Carmicino, F. C., **Toward advanced solid fuel for hybrid propulsion**, Space Propulsion Conference, San Sebastian 2010, May 3rd-6th, Spain

[3] Božić, O., Porrmann, D., Lancelle, D. M. and Hartwig, A., **Program AHRES and its Contribution to Assess Features and Current Limitations of Hybrid Rocket Propulsion**, 63th Congress of International Astronautical Federation, October 2012, Naples, Italy, IAC-12-C4.2.8

[4] Porrmann, D., Božić, O. and Lancelle, D. M., **Regression Rate Models versus Experimental Results for Hybrid Rocket Engines based on H_2O_2 and HTPB/Al,** 64st International Astronautical Congress (IAC), September 23 -27, 2013, Beijing, China

[5] Božić, O., Porrmann, D., Lancelle, D. M. and May, S., **The last Achievements by Development of a Rocket Grade Hydrogen Peroxide Catalyst Chamber with Flow Capacity of 1kg/s,** Conf. SPACE PROPULSION 2014, ST-RCS-85, May 19th – 22nd, 2014, Cologne, Germany

[6] Porrmann, D., Wilken, S., Božić, O. and Lancelle, D. M., **First Results of Regression Rate Measurements on Ultrasonic Basis,** Conf. SPACE PROPULSION 2014, May 19th – 22nd, 2014, Cologne, Germany

[7] Lancelle, D. M. and Božić, O., **Thermal Protection-, Aero-dynamics- and Control Simulation of an Electromagnetically Launched Projectile**, Electromagnetic Launch Symposium, July 1st -5th, 2014, San Diego, California, USA

[8] Dobrovoljski, M. V., **Жидкостньие ракетньие двигатели** (Židkostnye raketnye dvigateli), Издательство Машино-строение, Москва, 1968

[9] Poppe, G., **Hydraulic-pneumatic and internal ballistic characteristics of the AHREUS engine for the upper stage of the VLM launch vehicle**, Master thesis, Technische Universität Braunschweig & DLR Institute of Aerodynamics and Flow Technology, Braunschweig, July 2014

[10] May, S., **Numerical Simulation of Flow and Combustion inside the Reaction Chamber of the AHRES Hybrid Rocket Engine**, Master thesis, Technische Universität Braunschweig & DLR Institute of Aerodynamics and Flow Technology, Braunschweig, May 2014

[11] Koch, P., **Optimization of the solid grain geometries for hybrid and solid rocket engines**, Diploma thesis, Technische Universität Braunschweig & DLR Institute of Aerodynamics and Flow Technology, Braunschweig, May 2014

[12] Martin, F., Chapelle, A. and Lemaire, F., **Promising Space Transportations Using Hybrid Propulsion, Space Propulsion Conference**, San Sebastian 2010, May 3rd-6th, Spain

[13] Anthoine, J. and Prévost, M., **Hybrid propulsion: an overview of the ONERA activities**, 4th EUCASS, 2011, July 4th – 8th 2011, St. Petersburg, Russia, ID 429

[14] Calabro, M., **Overview on Hybrid Propulsion**, 3rd European Conference for Aero-Space Sciences – EUCASS, 6th - 9th July 2009, Versailles-Paris, France; Progress in Propulsion Physics, Vol.2, Edited by L. DeLuca et al., EUCASS advances in aerospace sciences book ser., Torus Press 2011, ISBN 978-2-7598-0673-7

[15] Raizberg, B. A., Erohin, B. T. and Samsonov, K. P., ***Основы Теории Рабочих Процессов в Ракетных Системах на Твердом Топливе***, Moscow, Издательство Машиностроение, 1972

[16] McBridge, B. J., Zehe, M. J. and Gordon, S., *NASA Glenn R.C.,* **Coefficients for Calculating Thermodynamic Properties of Individual Species,** Technical report, Cleveland, Ohio, National Aeronautics and Space Administration, Glenn Research Center, 2002

[17] May, S. and Božić, O., **Numerical Simulation of the Flow and Combustion inside the Reaction Chamber of the AHRES Hybrid Rocket Engine**, STAB Symposium, Munich, 4th -5th November 2014 (accepted paper)

[18] Merotto, L., Boiocchi, M., Carea, F., Colombo, G., Galfetti, L. and De Luca, L. T., **Experimental Investigation of Metallized Hybrid Rocket Fuels**,3rd EUCASS (European Conference for Aero-Space Sciences), Versailles, Paris, 6th -9th July 2009.

[19] Chiaverini, M. J., **Review of Solid-Fuel Regression Rate Behavior in Classical and Nonclassical Hybrid Rocket Motors**. In: Fundamentals of Hybrid Rocket Combustion and Propulsion. Ed. by Chiaverini, M. J. and Kuo, K. K.., Vol. 218. Progress in Astronautics and Aeronautics. Reston, Virginia: American Institute of Aeronautics und Astronautics, 2006, pp. 37–125, ISBN-13: 978-1-56347-703-4

[20] Chiaverini, M. J., Kuo, K. K., Peretz, A. and Harting, G. C., **Regression rate and heat transfer corre-lations for hybrid rocket combustion**, Journal of Propulsion and Power, Vol. 17, No. 1, pp. 99–110, 2001.

[21] Ziebland, H. and Parkinson, R. C., **Heat Transfer in Rocket Engines**, AGARDograph ,No. 148, AGARD-AG-148-71

[22] Božić, O., **Space Propulsion** (Raumfahrtantriebe), Lecture notes for university Master & Bachelor study course at the Technische Universität Braunschweig, 2014

[23] Le Digabel, S., **Algorithm 909: NOMAD: Nonlinear optimisation with the MADS algorithm**, ACM Transaction on Mathematical Software, Vol. 37, No. 4, pp. 1-15, 2011